Passivated ZnSe nanocrystals prepared by hydrothermal methods and their optical properties

Lingling Peng, Yuhua Wang*, Qizheng Dong and Zhaofeng Wang

Homogeneous ZnSe nanocrystals were prepared via surfactant-assisted hydrothermal method. Surfactants agent CTAB was used to control the particle morphology and the growth rate. The structure, morphology and optical properties of ZnSe nanocrystals have been investigated by XRD, TEM and luminescence spectroscopy. The results indicated that the size of ZnSe nanocrystals ranged from 3.0 nm to 5.0 nm with cubic zinc blende structure. ZnSe nanocrystals coated by CTAB were revealed high dispersibility and distribution under TEM. Compared to the bulk ZnSe, the absorption edges and photoluminescence peaks of ZnSe nanocrystals were blue shifted to higher energies due to the quantum confinement effect. The emission intensity was strengthened after coated CTAB compared to bare sample. This was mainly due to the surface passivation. Meanwhile, we simply explored the formation mechanism of ZnSe nanocrystal in hydrothermal system.

Semiconductor nanocrystals (NCs), or quantum dots (QDs), have been extensively studied due to their quantum confinement effects which exhibit unique size dependent electronic and optical properties [1,2]. Narrow and intensive emission spectra, continuous absorption bands, high chemical and photobleaching stability, and surface functionality are among the most attractive properties of these materials, which are not available from either bulk materials or isolated atoms. At present, synthetic procedures have been developed for a few group II-VI and III-V. As one of the Zn-based II-VI compounds, ZnSe is a direct band-gap semiconductor, with one room-temperature band-gap energy and an emission at 2.7 eV making it a potentially good material for blue-diode lasers and other photoelectronic devices [3-5]. It is known that ZnSe nanocrystal is interesting luminescent material in the blue to the ultra violet range due to quantum confinement effect and have been widely studied for its fundamental properties and potential use in technological applications. It is used as widely tunable for light emitting diodes (LED) [6-8] especially a very well succedaneum for biomedical labeling to replace some high toxicity nanomaterials such as CdS, CdSe and CdTe quantum dots. For higher quality and lower fabrication costs, a variety of physical and chemical techniques have been tested to produce materials in nanoscale with properties required by industries. Molecular beam epitaxy (MBE) [9] is one of the most normal methods. Other methods such as metal organic chemical vapor deposition (MOCVD) [10,11] and vapor phase epitaxy (VPE) [12,13] were also reported. However, all of these methods required special device and usually included toxic metal organic reagents as raw material [14]. It is believed that the most straightforward way to synthesize ZnSe is direct combination of element zinc and selenium at high temperature. Li et al has reported a successful fabrication of ZnSe by hydrothermal method in specific solvents such as pyridine which is virulent, so it must be synthesized at glove-box [15]. Hua Gong et al once reported analogy method at low-temperature and the products presented hollow microsphere and powder [16]. In hydrothermal syntheses, reaction time, temperature, and mole ratios of the precursors and solvent were very important to the

Department of Materials Science, School of Physical Science and Technology, Lanzhou University, Lanzhou 730000, PR China
*Corresponding author. E-mail: wyh@lzu.edu.cn

formation of nanocrystals. Low temperature, high concentration, and short reaction time minimized the crystal size. In this paper, monodisperse spherical ZnSe nanocrystals were synthesized, which showed low surface defect concentrations and good luminescence properties.

Experimental procedure

The starting materials were Se (99.95% A.R.), Zn (90% A.R.), NaOH (96% A.R.), and cetyl trimethy ammonium bromide (CTAB). 12 mol/L NaOH aqueous solutions was poured into a bunsen beaker, and then CTAB was added and magnetically stirred until the CTAB thoroughly dissolved. The solution was placed into a 30 ml Teflon-lined autoclave. Zn and Se metal powders were directly added into the autoclave, adjusting CTAB content to 0%, 5%, 10% (mol), and the ratio of Zn:Se = 1.5. The obtained suspension solution was kept at fixed concentration and filled about 60% of autoclave. The autoclave was then sealed and heated in an oven at a rate of $3°C$/min. After heat treatment at $150°C$ for 2 h, the autoclave was cooled to room temperature naturally. The products were viscous fluid, added some water and collected by centrifugal sedimentation, then washed with ionized water then absolute alcohol repeated. Finally, the solid power samples were dried under vacuum at $40°C$ in a drying chamber in the same prepared condition. The as-prepared solid powders were stored away from light because they were unstable and easily oxidized in air.

The crystal structure of the samples was examined by X-ray diffractometer (XRD) with Ni-filtered CuKα radiation at room temperature. The scanning speed and step for measurements were 3°/min, and 0.02° in the range of (2θ=10-80°). The size and shape of the samples were characterized by transmission electron microscopy (TEM). The optical properties sample was measured by LAMBDA 950 Uv-vis spectrometer (Perkin Elmer. PE) and the photoluminescence spectra under ultraviolet (UV) region were measured by a Xe lamp (FLS-920T) at room temperature.

Results and discussion

Figure 1 shows the XRD patterns for ZnSe NCs with different nominal content of CTAB at 0, 5, 10% and marked as A, B, C respectively. The result indicated that all products were single phase and no peaks characteristic of impurity phases were observed, which indexed to the phase of ZnSe with a cubic blende ZnSe (JCPDS card, No.05-0522, a=5.667 Å), The typical broadening of the three diffraction peaks were observed, which indicated that the size of the ZnSe was very small and three peaks

at 27.33°, 45.65° and 53.94° corresponded to the (111), (220) and (311) planes of cubic ZnSe, respectively. The average diameter of the ZnSe particles can be calculated using Scherer's formula:

$$d = k\lambda / \beta \cos\theta$$

Where λ is the wavelength of the X-rays and equals 1.54056 Å, k = 0.89, β is the half-peak width of the diffraction peak, and θ is the Bragg angle. The average diameter of the three samples was obtained according to above equation: A = 4.50 nm, B = 4.15 nm and C = 3.84 nm.

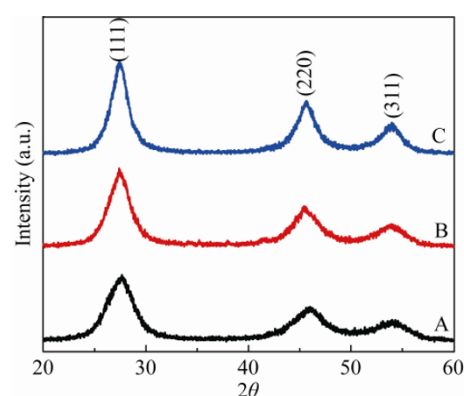Figure 2 gives the TEM image and electron diffraction

FIG. 1. XRD patterns of ZnSe nanocrystals: (A) without CTAB. (B) 5 mol% CTAB. (C) 10 mol% CTAB.

pattern of ZnSe NCs (The scale is 10 nm). The results showed that the nano size ZnSe particles produced by this method were spherical. Figure 2a was the sample without CTAB and we can observe that a majority of products were aggregated (sample A). Figure 2b displayed the image that CTAB concentration at 5% (sample B), compared to sample A, the particles were separated by adsorbed CTAB layer and the dispersibility of the particle was improved. The reason can be explained that CTAB is adsorbed on particle's surface in the solution. When the content of CTAB increased to 10% (Sample C), all particles were monodisperse and micelles were formed with the cation head pointing outwards in NaOH solution, so Zn^{2+} and Se^{2-} should react at the out-layers of the micelles to form ZnSe; that is why under TEM, hollow particles were observed. Moreover, the surface defects diminished and the surface of particles grew much more intact (see Fig. 2c). The images demonstrated that ZnSe nanocrystals with uniform and narrow-dispersed size distribution without aggregation were synthesized successfully. Electron diffraction technique confirmed the zinc-blende crystalline structure of the ZnSe nanocrystals with the (111),
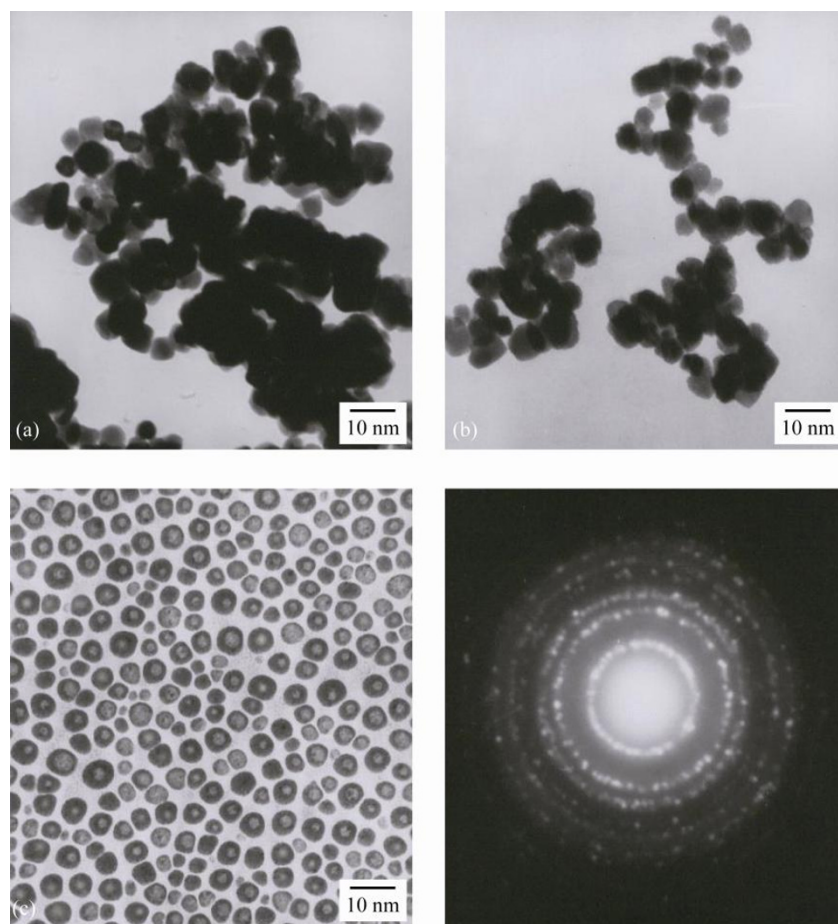
FIG. 2. TEM image and selected area electron diffraction pattern of ZnSe nanocrystals.

(220) and (311) diffraction rings in the electron diffraction pattern. According to Fig. 2, we conclude that the optimum content of CTAB was about 10%. It is reported that oleic acid played multiple roles in the formation of ZnSe NCs by acting not only as the reaction and shape controller but also as the stabilizing agent [17]. We can deduce that CTAB played similar roles by acting as the shape controller and growth speed indicator [18]. Surfactant CTAB can shielding the hydrophobic parts within the micellar interior, with the increases of surfactant concentration, the self-organization of micelles will produced [19]. It is indicated that another role of CTAB was to decrease the whole surface tension, making surface energy of the whole system reduce and improve the dispersibility of ZnSe nanocrystals. Figure 3 presents the histogram based on the TEM image (sample C), which revealed that the particle diameter ranged from 3.0~5.0 nm and the results was consistent with the calculated result measured by XRD.

Controlling the diameter is an important research objective for the NCs materials because diameter has a great effect on the luminescence properties. In the process of preparing ZnSe through hydrothermal synthesis employed Zn and Se as source materials and NaOH as hydrothermal medium, we concluded the forming mechanism as follows, when reactant concentration obviously increased, the solution was over-saturated, accelerating the velocity of nucleation and sharply increasing the quantity of the critical core. Meanwhile, reactant consumption also multiplied as there was no redundant reactant to consume; hence, the critical core growth was inhibited, as a result the grain size of product was smaller. At the same time, during the course of allegro formation of crystals, surface defects may increase by
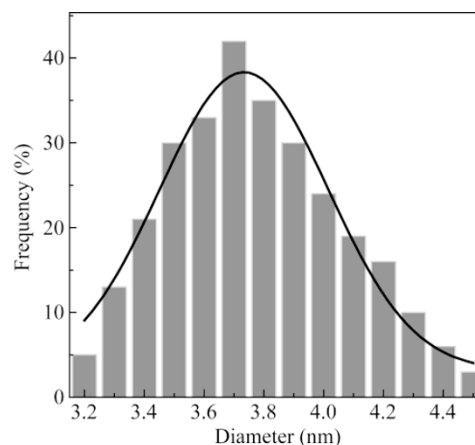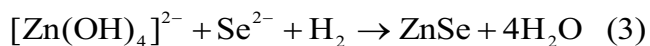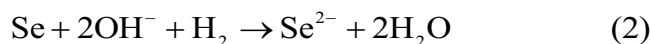

FIG. 3. Histogram based on the TEM (sample C) image.

the reason that there wasn't enough time for the surface atoms arrayed neatly. The result reflected that the surfactant CTAB sharply decreased surface defect, making surface smooth. Meanwhile, a growth mechanism of the ZnSe nanocrystals was proposed, the reactions in the hydrothermal solution can be formulated as the following:

$$Zn + 2H_2O + 2OH^- \rightarrow [Zn(OH)_4]^{2-} + H_2 \uparrow \quad (1)$$

$$Se + 2OH^- + H_2 \rightarrow Se^{2-} + 2H_2O \quad (2)$$

$$[Zn(OH)_4]^{2-} + Se^{2-} + H_2 \rightarrow ZnSe + 4H_2O \quad (3)$$

Zn and Se react with NaOH respectively and are dissolved in the hydrothermal solution. Then Se is reduced to Se^{2-} by H_2 generated in reaction (1). In order to completely reduce Se to Se^{2-}, the excessive Zn powders are used to generate enough H_2 and maintain sufficient reducing ambient in the hydrothermal system. That is the reason in the experiment of prepared ZnSe nanocrystals the ratio of Zn:Se is1.5.

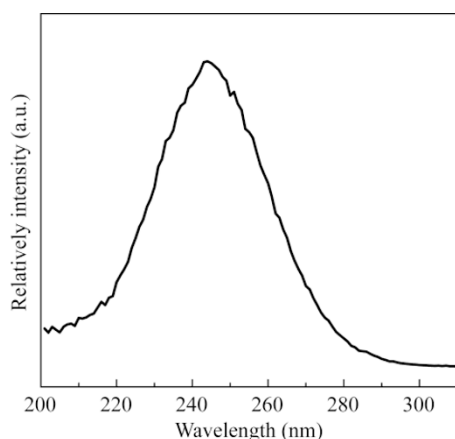Figure 4 gives the excitation spectrum of uncoated solid

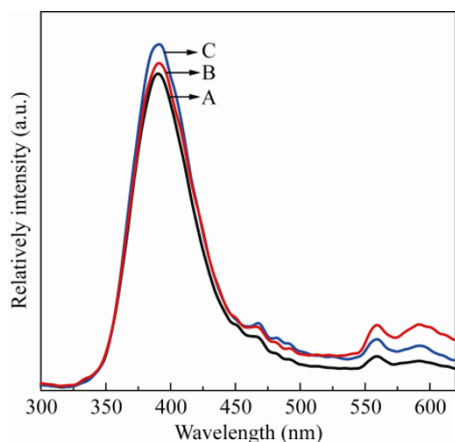FIG.4. The excitation spectrum of uncoated sample A.

FIG. 5. The emission spectra of ZnSe nanocrystals: (A) without CTAB. (B) 5 mol% CTAB. (C) 10 mol% CTAB

power sample (sample A) and Fig. 5 presents the emission spectra of ZnSe NCs, respectively. Monitored by 390 nm emission, a main broad band in the 200~ 280 nm range peaking at around 245 nm in the excitation spectrum which assigned to the higher excited state transitions of ZnSe NCs were observed [20] (In the measurement, we collected the spectrum range from 200 to 400nm. But after 300nm, there were no other absorption peak in spectra so the spectra were ending at 310nm in picture). As shown in Fig. 5, when excited by 245 nm, four emission bands from 300 to 650 nm with maxima at about 390 nm, 467 nm, 560 nm and 590 nm were observed. The first maximum at 390 nm is the exciton emission. The exciton emission can be attributed to the direct recombination of the electron-hole pair, an electron-hole pair will be generated when an intrinsic NC is excited by photons with energy higher than its band gap. The direct recombination of the electron-hole pair, typically being quantum confined in the case of nanocrystals [21], gives the well-known band edge emission at 390 nm which related to the higher excitonic states. The results were in accordance with the other results [22,23]. As a shoulder on a broad peak at 390 nm, the second band centered at 467 nm is attributed to band edge emission of few bigger particles. Two much broader peaks in the region of 550~650 nm were usually assigned to self-activated luminescence, probably as a result of some donor-acceptor pairs related to Zn-vacancy and interstitial states [24,25].

In ZnSe NCs surface, there were large quantity of dangling bonds which can induce defects and adatoms, in such circumstances, surface levels were formed because over half of atoms migrated to surface and became surface atoms which caused NCs have large specific surface area. Energy that excited to surface level was lower than that of to conduction band, so electrons were easily excited to surface level, and then came back to valence band to recombination with hole, causing surface state emission [26]. ''Self-purification'' mechanisms are often claimed to reasonably this effect, as the distance a defect must move to reach the surface of a nanocrystal is very small. Self-purification can be explained through energetic arguments and is an intrinsic property of defects in semiconductor nanocrystals. The formation energy of defects in nanocrystals increases as the size of the nanocrystals decreases [27]. The surface dangling bond states that lie within the band-gap typically quench the PL intensity. Surface passivation usually reduces the number of the surface dangling bonds [28]. It is observed that with the CTAB concentration increasing, the band edge emission intensity increased slightly because hackly surface was modified to some extent after being caped by CTAB.

Accordingly, a decrease in PL intensity was observed for nanocrystals with no CTAB owing to more defects in those nanocrystals (sample A). In this study, the CTAB capping layer was used not only as a passivation medium, but also to promote dispersivity of nanocrystals, which make the surface perfect and smooth, so band edge emission improved by reason that more electrons were excited to conduction band. The smooth surface and improved dispersity could be reflected in TEM. The luminescence peaks, covering a wavelength region of approximately 350~ 450 nm, are extremely narrow, the FWHM (full width at half maximum) of the all emission spectrum was under 40 nm. These values demonstrate clearly that a large size distribution is obtained [29].

Figure 6 displays the absorption spectra of ZnSe NCs (inset gives the optical absorbance with wavelength), the optical absorption increased sharply at wavelength 380 nm due to the direct transitions of the band gap of ZnSe and a slight wavelength shift from 380 nm to 375 nm was observed with the CTAB increased, this might be related to the decrease of grains, which also reflected that CTAB can control the particle growth rate. Meanwhile, there was a weak band appears at about 430~ 440 nm, we can interpreted it as non-uniformity of particles. From TEM image, we can see that not all particles were arranged form 3~ 5 nm, and the absorption band of which particles was in 380 nm. Beside, there were few bigger particles, whose absorption band would red-shifted, so we observed weak absorption, this results was in accordance with the emission spectrum. The quantum confinement effect can be qualitatively explained using the effective mass approximation (EMA), when the NCs size was smaller than exciton Bohr radius, the electrons and holes were independently confined, and Coulomb interaction was then a perturbation, so the electron–hole transition energy to the i th excited state of the NCs was determined by formula

$$\mathrm{E} = E_e + E_g = Eg + \frac{h^2 \pi^2}{2R^2}\left(\frac{1}{m_e} + \frac{1}{m_h}\right) - \frac{1.8e^2}{\varepsilon R}$$

Where h is Planck's constant; E_g is the band gap energy of ZnSe NCs, R is the radius of ZnSe NCs, m_e is the effective masses of electrons, m_h is the effective mass of holes, and ε is the dielectric constant or relative permittivity of ZnSe. The second term on the right hand side shows that the effective band gap is inversely proportional to R^2 and increases as size decreases. On the other hand, the last term in Eq indicates the Coulomb

interaction energy, which decreases the energy of electron-hole pair state [30]. Consequently, we could calculate the size of ZnSe NCs that was base on an infinite confinement spherical
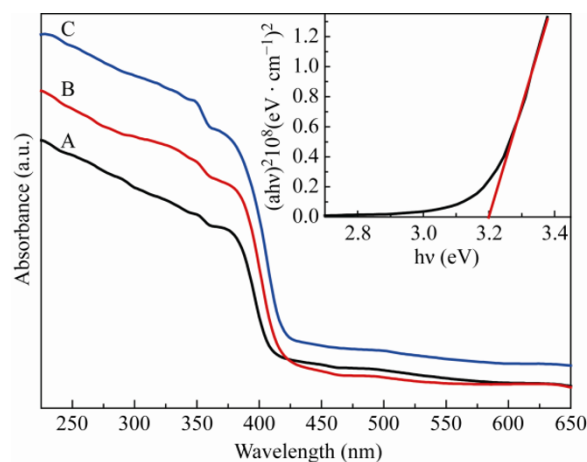

FIG. 6. UV-vis absorption spectra of ZnSe nanocrystals: (A) without CTAB. (B) 5 mol% CTAB. (C) 10 mol% CTAB, inset is plots of (αhv)2 vs hv of ZnSe nanocrystals

well potential model. The parameters used for the calculation were: $E_g = 2.7$ eV, $m_e = 0.16$ m_0, and $m_h = 0.75$ m_0 (m_0 is the mass of electron). Accordingly, considering the Coulomb interaction, the particle size was calculated ranges from 2.8 to 5.3 nm, in reasonable agreement with the XRD and TEM results. Figure 6 inset shows the $(\alpha hv)^2$ versus hv graph. The direct absorption band gap of the ZnSe nanoparticles can be determined by fitting the absorption data to the equation (as shown in the inset of Fig. 6)

$$\alpha = B(hv - Eg)^{1/2} / hv$$

In which hv is the photon energy, α is the absorption coefficient Eg is the absorption band gap and B is a constant relative to the material. The absorption coefficient can be obtained from the equation $\alpha = \dfrac{2.303A}{d}$ where A is the absorbance and d is the thickness of the sample. Extrapolation of these curves on energy axis for zero absorption coefficients, gives the value of optical band gap energy. The band gap was found to be 3.2 eV for sample which showed blue shift of 0.5 eV from the standard band gap for bulk ZnSe (2.7 eV) [31].

Conclusions

In summary, spherical, low surface defect, homogeneous distribution and luminescence ZnSe nanocrystals were successfully prepared by environment friendly method. The

ZnSe nanocrystals were stable with diameters ranging from 2.5 to 5.0 nm derived in this work. The emission peaks were at 390 nm, which was strengthened after being encapsulated by CTAB. The optical absorption studies showed that the ZnSe NCs has optical band gap of 3.2 eV. Finally, we believe this work will be guidance on the foundation study of nanocrystals luminescence.

References

1. Alivisatos. A. P, Science 271, 933 (1996). doi:10.1126/science.271.5251.933

2. Narayan Pradhan and Xiaogang Peng, J. American Chem. S. 129, 3339 (2007). doi:10.1021/ja068360v

3. Nikolai P. Osipovich, Alexey Shavel, Sergey K. Poznyak, Nikolai Gaponik and Alexander Eychmu1ller, J. Phys. Chem. B 110, 19233 (2006). doi:10.1021/ jp063104q

4. Acharya. S, Panda. A. B, Efrima. S and Golan. Y, Adv. Mater. 19, 1105 (2007). doi:10.100 2/adma.200602057

5. F. T. Quinlan, J. Kuther, W. Tremel, W. Knoll, S. Risbud and P. Stroeve, Langmuir 16, 4049. (2000). doi:10.1021/la9909291

6. Hsueh Shih Chen, Shian Jy, Jassy Wang, Chun Jeu Lo and Jim Yong Chi, Appl. Phys. L. 86, 1905 (2005). doi:10.1063/1.1886894

7. Takao Nakamura, Shinsuke Fujiwara, Hiroki Mori, Koji Katayama and Jpn. J. Appl. Phys. 43, 1287 (2004). doi:10.1143/JJAP.43.1287

8. Wen Ray Chen and Chien Jung Huang, Photo. Tech. L. 16, 5 (2004). doi: 10.1109/LPT.2004.826116

9. E. Roventa, G. Alexe, M. Schowalter, R. Kroger, D. Hommel and A. Rosenauer, Phys. S. Solidi. (c). 3, 887 (2006). doi: 10.1002/pssc.200564694

10. X. T. Zhang, Z. Liu, Y. P. Leung, Quan Li and S. K. Hark, Appl. Phys. L. 83, 5533 (2003). doi:10.1063/1.1638633

11. M. C. Harris Liao, Y. H. Chang, Y. F. Chen, J. W. Hsu , J. M. Lin and W. C. Chou, App. Phys. L. 70, 2256 (1997). doi:10.1063/1.118831

12. Tishchenko V. V, Bondar N. V, Kovalenko A. V, Halsall M. P and Lilley P, Sup. Micro. 24, 143(1998). doi:10.1006/spmi.1998.0575

13. T. Tawara, S. Tanaka, H. Kumano and I. Suemune, App. Phys. L. 75, 235 (1999). doi:10.1063/1.124333

14. P. Davide Cozzoli, Liberato Manna, M. Lucia Curri, Stefan Kudera, Cinzia Giannini, Marinella Striccoli and Angela Agostiano, Chem. Mat. 17, 1296 (2005). doi:10.1021/cm047874v

15. Yadong Li, Hongwei Liao, Yi Ding, Yue Fan, Yue Zhang and Yitai Qian, Inorg. Chem. 38, 1382 (1999). doi:10.1021/ic980878f

16. Hua Gong, Hui Huang, Liang Ding, Minqiang Wangc and Kaiping Liu, J. Crys. G. 288, 96 (2006). doi:10.1016/j.jcrysgro.2005.12.030

17. Yang Jiao, Dabin Yu, Zirong Wang, Kun Tang and Xiaoquan Sun, Mat. L. 61, 1541 (2007). doi:10.1016/j.matlet.2006.07.103

18. Chatterjee, A. Priyam, S. C. Bhattacharya and A. Saha, Colloid. Surf. 297, 258 (2007). doi:10.1016/j.colsurfa.2006.10.053

19. Jeffrey Brinker, Yunfeng Lu, Alan Sellinger and Hongyou Fan, Advanced materials 11, 579 (1999). doi: 10.1002/(SICI)1521-4095(199905)

20. V. V. Nikesh, Amit D. Lad, Seiji Kimura, Shinji Nozaki and Shailaja Mahamuni, J. App. Phys. 100, 113520-1 (2006). doi:10.1063/1.2397289

21. L. E Brus, J. Chem. Phys, 79, 5566 (1983). doi:10.1063/1.445676

22. Yuangang Zheng, Zichao Yang and Jackie Y. Ying, Adv. Mater. 19, 1475 (2007). doi: 10.1002/ adma.200601939

23. Qi Qiu, TracyHeckler, JunWang, BingC.Mei and T. J. Mountziaris, J. Lum. 130, 1504 (2010). doi:10.1016/j.jlumin.2010.03.020

24. J. Q. Hu, Y. Bando and D. Golberg, Small 1, 95 (2005). doi:10.1002/smll.200400013

25. Y. Jiang, X. M. Meng, W. C. Yiu, J. Liu, J. X. Ding, C. S. Lee and S. T. Lee, J. Phys. Chem.B. 108, 2784 (2004). doi:10.1021/jp035595+

26. Liu Meng, Zhang Jia and Chi Yan Hua, Ch. J. Inorg Chem. 22, 651 (2006). doi: CNKI:SUN:WJHX.0.2006-04-010

27. Gustavo M. Dalpian and James R. Chelikowsky, Phys. Rev. Lett. 96, 226802 (2006). doi:10.1103/PhysRevLett.96.226802

28. Hsueh Shih Chena, Shian Jy Jassy Wang, Chun Jeu Lo and Jim Yong Chi, App. Phys. L. 86, 131905 (2005). doi:10.1063/1.1886894

29. P. Reiss, G. Quemard, S. Carayon, J. Bleuse, F. Chandezon and A. Pron, Ma. Chem. Phys. 84, 10 (2004). doi:10.1016/j.matchemphys.2003.11.002

30. L. E. Brus, J. Chem. Phys. 80. 4403 (1984). doi:10.1063/1.447218

31. P. Pramanik and S. Biswas, J. Solid. State Chem. 65, 145 (1986). doi:10.1016/0022-4596(86)90098-8